

## Constraining Binding Hot Spots: NMR and Molecular Dynamics Simulations Provide a Structural Explanation for Enthalpy–Entropy Compensation in SH2–Ligand Binding

Joshua M. Ward,<sup>†</sup> Nina M. Gorenstein,<sup>†</sup> Jianhua Tian,<sup>‡</sup> Stephen F. Martin,<sup>‡</sup> and Carol Beth Post<sup>\*,†</sup>

*Department of Medicinal Chemistry, Markey Center for Structural Biology, and Purdue Cancer Center, Purdue University, West Lafayette, Indiana 47907, and Department of Chemistry and Biochemistry and The Institute of Cellular and Molecular Biology, The University of Texas, Austin, Texas 78712*

Received December 14, 2009; E-mail: cbp@purdue.edu

**Abstract:** NMR spectroscopy and molecular dynamics (MD) simulations were used to probe the structure and dynamics of complexes of three phosphotyrosine-derived peptides with the Src SH2 domain in an effort to uncover a structural explanation for enthalpy–entropy compensation observed in the binding thermodynamics. The series of phosphotyrosine peptide derivatives comprises the natural pYEEI Src SH2 ligand, a constrained mimic, in which the phosphotyrosine (pY) residue is preorganized in the bound conformation for the purpose of gaining an entropic advantage to binding, and a flexible analogue of the constrained mimic. The expected gain in binding entropy of the constrained mimic was realized; however, a balancing loss in binding enthalpy was also observed that could not be rationalized from the crystallographic structures. We examined protein dynamics to evaluate whether the observed enthalpic penalty might be the result of effects arising from altered motions in the complex. <sup>15</sup>N-relaxation studies and positional fluctuations from molecular dynamics indicate that the main-chain dynamics of the protein show little variation among the three complexes. Root mean squared (rms) coordinate deviations vary by less than 1.5 Å for all non-hydrogen atoms for the crystal structures and in the ensemble average structures calculated from the simulations. In contrast to this striking similarity in the structures and dynamics, there are a number of large chemical shift differences from residues across the binding interface, but particularly from key Src SH2 residues that interact with pY, the “hot spot” residue, which contributes about one-half of the binding free energy. Rank-order correlations between chemical shifts and ligand binding enthalpy for several pY-binding residues, coupled with available mutagenesis and calorimetric data, suggest that subtle structural perturbations (<1 Å) from the conformational constraint of the pY residue sufficiently alter the geometry of enthalpically critical interactions in the binding pocket to cause the loss of binding enthalpy, leading to the observed enthalpy–entropy compensation. We find no evidence to support the premise that enthalpy–entropy compensation is an inherent property and conclude that preorganization of Src SH2 ligand residues involved in binding hot spots may eventuate in suboptimal interactions with the domain. We propose that introducing constraints elsewhere in the ligand could minimize enthalpy–entropy compensation effects. The results illustrate the utility of the NMR chemical shift to highlight small, but energetically significant, perturbations in structure that might otherwise go unnoticed in an apparently rigid protein.

### Introduction

Structure-based drug design is an important application of structural biology studies. Using the atomic structure of a biological receptor complexed with a ligand, one should ideally be able to characterize the binding interface and propose specific modifications to the ligand that would enhance the free energy for association. However, this process is often fraught with difficulty in practice, as changes intended to optimize either the enthalpy or the entropy of binding are often met with unanticipated energetic results.<sup>1–3</sup>

The structure of a small molecule may be modified in a number of ways toward improving its potency for a biological target. One common tactic involves preorganizing the ligand in the conformation it adopts upon binding, commonly referred to as the biologically active conformation.<sup>4–6</sup> This practice owes its origin to the fact that there is an entropic penalty associated with restricting the motion of a flexible molecule when it binds

<sup>†</sup> Purdue University.

<sup>‡</sup> The University of Texas.

(1) Lazaridis, T. *Curr. Org. Chem.* **2002**, *6*, 1319–1332.

(2) Gohlke, H.; Klebe, G. *Angew. Chem., Int. Ed.* **2002**, *41*, 2645–2676.

(3) Henriques, D. A.; Ladbury, J. E. *Arch. Biochem. Biophys.* **2001**, *390*, 158–168.

(4) Mann, A. In *The Practice of Medicinal Chemistry*, 2nd ed.; Wermuth, C. G., Ed.; Academic Press: London, UK, 2003; pp 233–250.

(5) Nakanishi, H.; Kahn, M. Design of Peptidomimetics. In *The Practice of Medicinal Chemistry*, 2nd ed.; Wermuth, C. G., Ed.; Academic Press: London, UK, 2003; pp 477–500.

(6) Loughlin, W. A.; Tyndall, J. D. A.; Glenn, M. P.; Fairlie, D. P. *Chem. Rev.* **2004**, *104*, 6085–6118.

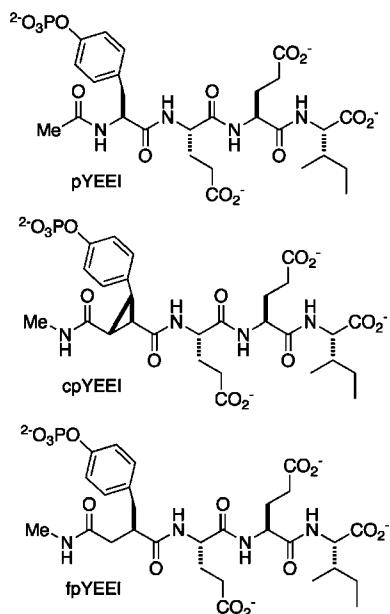


**Figure 1.** Schematic of the canonical (pYEEI), constrained (cpYEEI), and flexible (fpYEEI) ligands studied in this investigation. pY denotes the natural phosphorylated tyrosine residue. cpY denotes the trisubstituted cyclopropane replacement used to mimic the bound state conformation of pY. fpY denotes the flexible control replacement that has the same number of heavy atoms as cpY and is designed to account for the rearrangement of the hydrogen-bonding capacity between the pY and cpY residues.

to a protein. Accordingly, constraining a flexible molecule in its biologically active conformation is expected to reduce the magnitude of this entropic penalty, thereby providing a relatively favorable contribution to the binding free energy.<sup>7–9</sup> Calorimetric studies have established that a more favorable binding entropy can be realized by preorganization, although recent accounts have revealed that ligand preorganization does not necessarily lead to an entropic advantage in binding.<sup>10–12</sup>

The effects of ligand preorganization upon the binding energetics of a set of constrained and flexible analogues of the canonical pYEEI peptide for the pp60 v-Src SH2 (Src SH2) domain have been examined.<sup>13,14</sup> In the constrained analogue (cpYEEI), a trisubstituted cyclopropyl moiety was used as a rigid replacement of the pY residue (Figure 1). Modeling suggested that this rigid replacement mimicked the conformation of the pY side-chain that is observed in structures of phosphotyrosine-derived peptides bound to this and other SH2 domains.<sup>15–17</sup> Because pYEEI and cpYEEI do not have the same number of heavy atoms, the appropriate flexible control for cpYEEI is fpYEEI, wherein a benzyl succinate moiety serves

as a flexible replacement of the pY residue (Figure 1). Both cpYEEI and fpYEEI have the same number and type of heavy atoms, the same functional groups, and the same number of hydrogen-bond donors and acceptors, so it was reasoned that desolvation effects for each would be similar. The binding thermodynamics of these three ligands for the recombinant Src SH2 domain were determined using isothermal titration calorimetry (ITC). It was found that the constrained pseudopeptide, cpYEEI, exhibited a binding entropy about 7 cal mol<sup>-1</sup> K<sup>-1</sup> more favorable (positive  $\Delta\Delta S^\circ$ ) than its tetrapeptide counterpart pYEEI and nearly 9 cal mol<sup>-1</sup> K<sup>-1</sup> more favorable than its flexible control fpYEEI. Nevertheless, the relative binding enthalpy of cpYEEI was about 1.5 kcal mol<sup>-1</sup> less favorable (positive  $\Delta\Delta H^\circ$ ) than pYEEI and 2.7 kcal mol<sup>-1</sup> less favorable than fpYEEI. We thus observed the expected entropic advantage attending preorganization of the cpY residue relative to pY and the flexible replacement fpY, but an enthalpic penalty offset this entropic gain in both cases. The end result from this observed enthalpy–entropy compensation was that the binding affinity of cpYEEI was only slightly higher than that of pYEEI and slightly lower than that of fpYEEI, and the relative binding enthalpies for the three Src SH2 complexes are most favorable for the fpY pseudopeptide and least favorable for the cpY pseudopeptide.

Enthalpy–entropy compensation has been a topic of discussion in the literature for many years.<sup>18–22</sup> Because of its prevalence in biological systems,<sup>18,21,23</sup> enthalpy–entropy compensation has been proposed to be an inherent property of aqueous solution associated with the reorganization of hydrogen-bonding patterns in the hydration shells of proteins and small molecules.<sup>18</sup> On the other hand, this view has been countered by theoretical derivations arguing that such a correlation is not a fundamental thermodynamic requirement,<sup>19,21,22</sup> and there are some examples of noncompensating systems in which anticorrelation between enthalpy and entropy serves to amplify gains in the binding free energy.<sup>21,24</sup> Despite the body of literature on the subject, a full understanding of compensation mechanisms in protein–ligand interactions is lacking. Such an understanding could prove beneficial to rational drug design if one knew how to minimize enthalpy–entropy compensation to take advantage of one free energy component, and thus the physical basis for the differences in the enthalpy of binding among the three Src SH2 complexes is examined here.

Less favorable enthalpy of binding in the case of Src SH2 by a pseudopeptide could, of course, result from an altered binding conformation relative to a canonical peptide ligand. To identify a potential structural basis for the compensation observed in this series of Src SH2 binding ligands, crystal

- (7) Khan, A. R.; Parrish, J. C.; Fraser, M. E.; Smith, W. W.; Bartlett, P. A.; James, M. N. G. *Biochemistry* **1998**, *37*, 16839–16845.
- (8) Schneider, H.-J. In *Protein–Ligand Interactions: From Molecular Recognition to Drug Design*; Böhm, H.-J., Schneider, G., Eds.; Wiley-VCH: Weinheim, 2003; pp 21–50.
- (9) Reichelt, A.; Martin, S. F. *Acc. Chem. Res.* **2006**, *39*, 433–442.
- (10) Benfield, A. P.; Teresk, M. G.; Plake, H. R.; Delorbe, J. E.; Millsbaugh, L. E.; Martin, S. F. *Angew. Chem., Int. Ed.* **2006**, *45*, 6830–6835.
- (11) DeLorbe, J. E.; Clements, J. H.; Teresk, M. G.; Benfield, A. P.; Plake, H. R.; Millsbaugh, L. E.; Martin, S. F. *J. Am. Chem. Soc.* **2009**, *131*, 16758–167570.
- (12) Udagamasooriya, D. G.; Spaller, M. R. *Biopolymers* **2008**, *8*, 653–667.
- (13) Davidson, J. P.; Martin, S. F. *Tetrahedron Lett.* **2000**, *41*, 9459–9464.
- (14) Davidson, J. P.; Lubman, O.; Rose, T.; Waksman, G.; Martin, S. F. *J. Am. Chem. Soc.* **2002**, *124*, 205–215.
- (15) Waksman, G.; Shoelson, S. E.; Pant, N.; Cowburn, D.; Kuriyan, J. *Cell* **1993**, *72*, 779–790.

- (16) Rahuel, J.; Gay, B.; Erdmann, D.; Strauss, A.; Garcia-Echeverria, C.; Furet, P.; Caravatti, G.; Fretz, H.; Schoepfer, J.; Grütter, M. G. *Nat. Struct. Biol.* **1996**, *3*, 586–589.
- (17) Waksman, G.; Kumaran, S.; Lubman, O. *Expert Rev. Mol. Med.* **2004**, *6*, 1–18, and references therein.
- (18) Lumry, R.; Rajender, S. *Biopolymers* **1970**, *9*, 1125–1227.
- (19) Dunitz, J. D. *Chem. Biol.* **1995**, *2*, 709–712.
- (20) Searle, M. S.; Westwell, M. S.; Williams, D. H. *J. Chem. Soc., Perkin Trans. 2* **1995**, *1995*, 141–151.
- (21) Gallicchio, E.; Kubo, M. M.; Levy, R. M. *J. Am. Chem. Soc.* **1998**, *120*, 4526–4527.
- (22) Sharp, K. *Protein Sci.* **2001**, *10*, 661–667.
- (23) Gilli, P.; Ferretti, V.; Gilli, G.; Borea, P. A. *J. Phys. Chem.* **1994**, *98*, 1515–1518.
- (24) Ford, D. M. *J. Am. Chem. Soc.* **2005**, *127*, 16167–16170. Post, C. B.; Dobson, C. M.; Karplus, M. In *Computer Modeling of Carbohydrate Molecules*; French, A. D., Brady, J. W., Eds.; American Chemical Society: Washington, DC, 1990; pp 377–388.

structures of Src SH2 in complex with the cpYEEI pseudopeptide (Figure 1) and a canonical peptide were compared.<sup>14</sup> It was not possible to obtain a structure of the Src SH2 complex with fpYEEI. The rmsd between the complex with cpYEEI and that with the canonical peptide was approximately 1 Å for protein main-chain atoms and within 1.5 Å over all heavy atoms. Because differences between the structures of the two complexes are comparable to the differences between multiple copies of a complex in each asymmetric unit, no significant structural perturbations that adequately explain the compensation<sup>14</sup> could be identified.

The lack of a significant structural difference observed between the crystallographic models for the Src SH2 complexes with pYEEI and cpYEEI, and reasoning that desolvation effects would be similar for the pseudopeptides, raises the question of whether variations in internal dynamics associated with the cyclopropyl moiety exist and are the cause for less favorable interaction energy in the cpYEEI complex. If so, then a direct link between the observed loss in enthalpy and the gain in entropy would be established, suggesting that enthalpy–entropy compensation is inherent to binding Src SH2. In the presence of certain conformational motions, dynamic averaging over the thermal distribution of protein–ligand conformations was shown in an MD study to be important in determining the interaction energies; the relative energies for protein–ligand interactions estimated from the average structure were shown to differ from the relative values determined from the ensemble-averaged energy,<sup>24</sup> which is the thermodynamically relevant quantity. It is reasonable that restricted motion imposed by the conformational constraint of cpYEEI could affect the ensemble averaging in a manner that weakens intermolecular interactions without significantly affecting the average structure. A wide body of evidence demonstrates the importance of thermal motions to protein function and the need to include conformational fluctuations in characterizing protein–ligand interactions.<sup>25–29</sup> While X-ray crystallography gives accurate three-dimensional structures of proteins, it provides limited information on dynamics, so that possible energetic differences that result from dynamic averaging over the fluctuations about the average structure would be invisible by crystallography. On the other hand, NMR relaxation and molecular dynamics simulations, which have been valuable for elucidating the effects from internal fluctuations and conformational entropy of proteins to molecular association,<sup>1,25,30–33</sup> can contribute to understanding differences in internal dynamics and enthalpy of proteins in a manner that is not apparent from an average structure.

In this light, we probed the differences between the pYEEI, cpYEEI, and fpYEEI complexes of Src SH2 by NMR and computer simulation. Positional fluctuations were examined to determine if the enthalpic loss in the Src SH2–cpYEEI complex

might arise from restricted motion in the complex that could result in the observed enthalpy–entropy compensation. NMR chemical shift analysis was also used to probe structural differences between the solution structures of the three SH2–peptide complexes.<sup>34</sup>

## Materials and Methods

### Protein Expression, Purification, and Sample Preparation.

The canonical pYEEI tetrapeptide was purchased with an acetylated N-terminus and unblocked C-terminus (SynPep). The cpYEEI and fpYEEI pseudopeptide derivatives were synthesized as previously described.<sup>13</sup> Protein was expressed and purified in a manner similar to previously reported protocols.<sup>35,36</sup> A construct consisting of residues 144–249 of the pp60 v-Src tyrosine kinase (UniProt P00524) that comprise the SH2 domain (Src SH2) was cloned into a pET30b expression vector (Novagen) at the *Nde*I and *Bam*HI restriction sites. Protein was overexpressed in Rosetta2 (DE3) *E. coli* (Novagen) grown on M9 minimal media with 1 g/L <sup>15</sup>N-labeled NH<sub>4</sub>Cl as the sole nitrogen source and at least 2 g/L glucose as the sole carbon source, unlabeled or uniformly <sup>13</sup>C-labeled as required. Induction was initiated with 0.2 mM IPTG after incubating for 16–20 h at 22 °C.

Cells were lysed using a French press in 20 mM (Na)HEPES, pH 7.5, 5 mM DTT, 1 mM EDTA, 0.2 mM PMSF, and 0.02% NaN<sub>3</sub>. After ultracentrifugation, the supernatant was loaded onto a 5 mL cation exchange HiTrap SP column (GE) that had been equilibrated with the same buffer. The protein was eluted with a 0–0.5 M NaCl gradient in the same buffer. Src SH2 containing fractions were pooled and concentrated to ~2 mL using Amicon-Ultra-15 concentrators (Millipore) with 3 kDa molecular weight cutoff (MWCO) prior to final purification by gel filtration (Superdex 75 16/60, Pharmacia) using 20 mM (Na)HEPES, pH 7.5, 5 mM DTT, 1 mM EDTA, 350 mM NaCl, and 0.02% NaN<sub>3</sub>.

NMR experiments were conducted in 50 mM Na acetate, pH 5.5, 100 mM NaCl, 5 mM TCEP, and 0.02% NaN<sub>3</sub> (from Xu et al.<sup>36</sup> with minor variations). Pooled fractions containing Src SH2 were dialyzed against the NMR buffer (2–3 times, at least 6 h each time) using Snake Skin dialysis membranes with 3.5 kDa MWCO (Pierce). Peptides were dissolved in 100 μL of NMR buffer. After adjusting the pH to ~5.5 with aqueous NaOH, the peptide stock was dialyzed alongside the protein using 100 Da MWCO membranes (Harvard Bioscience). Protein was concentrated to 1–1.8 mM using 3 kDa MWCO concentrators (Millipore). NMR samples in 90%/10% H<sub>2</sub>O/D<sub>2</sub>O were prepared by combining appropriate proportions of protein, peptide stock, and D<sub>2</sub>O. Concentrations were measured by UV absorbance at 280 nm with an extinction coefficient of 14 700 M<sup>-1</sup> cm<sup>-1</sup> for protein, and 775 M<sup>-1</sup> cm<sup>-1</sup> at 268 nm for the peptides.<sup>14</sup>

**NMR Spectroscopy.** NMR spectra were acquired at 298 K on a Bruker Avance III spectrometer operating at 800 MHz and a TXI triple resonance probe using standard pulse sequences from the Bruker pulse sequence library. Spectra were processed with NMRPipe<sup>37</sup> and viewed with Sparky.<sup>38</sup> Samples contained approximately 1 mM Src SH2 domain and 5 mM ligand to ensure saturation of the bound state conformation of each complex, as determined by titrations monitored by <sup>15</sup>N HSQC. Initial assignments based on the published values for the Src SH2–pYEEI

(25) Karplus, M.; McCammon, J. A. *Nat. Struct. Biol.* **2002**, *9*, 646–652.

(26) Daniel, R.; Dunn, R.; Finney, J.; Smith, J. *Annu. Rev. Biophys. Biomol. Struct.* **2003**, *32*, 69–92.

(27) Kay, L. *Biochem. Cell. Biol.* **1998**, *76*, 145–152.

(28) Mittermaier, A.; Kay, L. *Science* **2006**, *312*, 224–228.

(29) Spyropoulos, L.; Sykes, B. D. *Curr. Opin. Struct. Biol.* **2001**, *11*, 555–559.

(30) Karplus, M.; Ichiye, T.; Pettit, B. M. *Biophys. J.* **1987**, *52*, 1083–1085.

(31) Brooks, B.; Karplus, M. *Proc. Natl. Acad. Sci. U.S.A.* **1983**, *80*, 6571–6575.

(32) Tidor, B.; Karplus, M. *J. Mol. Biol.* **1994**, *238*, 405–414.

(33) Stöckmann, H.; Bronowska, A.; Syme, N. R.; Thompson, G. S.; Kalverda, A. P.; Warriner, S. L.; Homans, S. W. *J. Am. Chem. Soc.* **2008**, *130*, 12420–12426.

(34) Günther, U. L.; Liu, Y.; Sanford, D.; Bachovchin, W. W.; Schaffhausen, B. *Biochemistry* **1996**, *35*, 15570–15581.

(35) Waksman, G.; Kominos, D.; Robertson, S. C.; Pant, N.; Baltimore, D.; Birge, R. B.; Cowburn, D.; Hanafusa, H.; Mayer, B. J.; Overduin, M.; Resh, M. D.; Rios, C. B.; Silverman, L.; Kuriyan, J. *Nature* **1992**, *358*, 646–653.

(36) Xu, R. X.; Word, J. M.; Davis, D. G.; Rink, M. J.; Willard, D. H.; Gampe, R. T. *Biochemistry* **1995**, *34*, 2107–2121.

(37) Delaglio, F.; Grzesiek, S.; Vuister, G. W.; Zhu, G.; Pfeifer, J.; Bax, A. *J. Biomol. NMR* **1995**, *6*, 277–293.

(38) Kneller, D. G.; Kuntz, I. D. *J. Cell. Biochem.* **1993**, *53*, 254–254.

complex<sup>36</sup> were confirmed with the MARS program<sup>39</sup> using data from standard HNCACB and CBCACONH triple resonance experiments.<sup>40</sup> Because of large changes in chemical shift, the main-chain experiments were conducted and full main-chain assignment performed for all four samples (unbound SH2, SH2–pYEEI, SH2–cpYEEI, and SH2–fpYEEI). The 800 MHz spectra were well resolved, allowing main-chain assignment of all nonproline residues.

During the assignment process, the peaks of E178 NH and R175 NεHe, which were assigned on the basis of published values,<sup>36,41</sup> showed rank-order correlation with binding enthalpy. Both residues are located in the pY-binding pocket and are directly involved with coordination of the phosphoryl group on the ligand. It was assumed, therefore, that the trend in the chemical shifts is related to the deshielding effect of the negatively charged phosphate group and the stability of its interaction with the residues. This assumption, which is further supported throughout the results and discussion, led to the assignment of peaks for the R175 NηHη side-chain atoms that bind the phosphoryl moiety of the ligand. After accounting for the main-chain amides of all nonproline residues and the side-chain values available in the published shifts, a group of unassigned peaks remained that were located in the region of the spectra populated by the arginine and histidine side-chain peaks and followed the same rank-order trend with enthalpy. The chemical shift values fall within the statistical range compiled for proteins in the BMRB and have proton chemical shifts similar to R160 NηHη, based on the reported values for the c-Src SH2–pYEEI complex by Xu et al.<sup>36</sup>

Standard pulse sequences were used to measure the main-chain <sup>15</sup>N relaxation rates,<sup>42</sup> with interscan relaxation delays of 2 s for all experiments and a 2 s saturation time for the NOE experiments. Delay times of 10, 35 (in duplicate), 50, 175, 375, 550 (in duplicate), 750, 1000, and 1400 ms were employed for *T*<sub>1</sub> measurements. CPMG delays of 16.3, 32.6 (in duplicate), 48.9, 65.2, 81.5, 97.9 (in duplicate), 114.2, and 130.5 ms were employed for *T*<sub>2</sub> measurements. Exponential decay times were fit to peak heights in Sparky. Chemical shift perturbations (CSPs) and chemical shift differences (CSDs) were calculated from sensitivity-enhanced <sup>1</sup>H–<sup>15</sup>N HSQC spectra<sup>43</sup> according to:<sup>44</sup>

$$X = \sqrt{0.5[\Delta\delta_{\text{H}}^2 + (0.2\Delta\delta_{\text{N}}^2)]^2} \quad (1)$$

$$X = \begin{cases} \text{CSP: } \Delta\delta = \delta_{\text{complex}} - \delta_{\text{unbound}} \\ \text{CSD: } \Delta\delta = \delta_{\text{complex2}} - \delta_{\text{complex1}} \end{cases}$$

**Molecular Dynamics Simulations.** Dynamics simulations were calculated with CHARMM<sup>45</sup> using the CHARMM27 all-atom force field<sup>46</sup> with CMAP main-chain dihedral correction.<sup>47</sup> Supplementary topology and parameters for the cyclopropyl moiety (Supporting Information) were generated according to the standard CHARMM force field parametrization methodology.<sup>46</sup> Equilibrium geometries and reference vibrational data for this moiety were obtained from

the NIST CCCBDB database.<sup>48</sup> Reference energy curves from HF/6-31 g\*\* ab initio dihedral optimizations of model compounds were used to parametrize the torsional parameters for rotation about the Cβ–Cγ bond (χ<sub>1</sub> rotamer) and cyclopropyl–carbonyl “main-chain” bonds in cpY. Parameters for the fpY residue were assigned by analogy to existing force field values.

Initial coordinates for the complex models were taken from the three chains of the Src SH2–pYEEI crystal structure (PDB code 1SPS<sup>49</sup>) and the two chains of the Src SH2–cpYEEI crystal structure (PDB code 1IS0<sup>13</sup>). For each complex being simulated, the peptide was alchemically mutated to obtain the desired model pseudopeptide in each case, yielding five sets of starting coordinates. To increase the efficiency of conformational sampling, two independent simulations using different initial velocities were initiated from each set of starting coordinates to yield 10 independent simulations of each complex.<sup>50</sup>

Solutes were solvated with a truncated octahedral water box of TIP3 water molecules with box edges at least 14 Å from the solute. Nonbonded lists were generated with a 14 Å cutoff, and electrostatic interactions up to 12 Å were treated with a shifted potential and particle mesh Ewald summation method during the dynamics. Bond lengths to hydrogen atoms were constrained with SHAKE. Dynamics were performed using a leapfrog integrator, time step of 1 fs, and constant pressure and temperature (CPT) routine using a reference pressure of 1 atm and piston mass constant of 500 amu. Hoover temperature control was employed with a temperature bath of 298 K and thermal piston constant of 1000 kcal ps<sup>2</sup> mol<sup>–1</sup>. Simulations were equilibrated for 500 ps, after which time all simulations were deemed reasonably energetically stable and displayed asymptotic rmsd time series relative to initial coordinates. Production runs of 1 ns were calculated for each simulation, with coordinates saved every 1 ps for a total of 10 ns of trajectory (10 000 snapshots) per complex. Dynamic properties were evaluated from this combined 10 ns pseudotrajectory. Average structures were calculated from the combined set and subjected to 500 steps of steepest descent minimization to remove severe steric clashes. Main-chain chemical shifts were calculated from these structures using Sparta.<sup>51</sup>

Hydrogen-bond analysis was performed with CHARMM's coordinate manipulation commands. For each frame in the trajectory, a hydrogen bond between a hydrogen-bond donor (D) and acceptor (A) was considered to be intact<sup>52</sup> if the D–A distance was less than 2.4 Å and the D–H···A angle was 120°–180°. Two-dimensional histograms for geometric analyses were calculated using 4° bins over a range of –180° to 180° for dihedral angles, and 0.5 Å bins over a range of 1–6 Å for interatomic distances.

Individual contributions of groups of water molecules to the energy of a Src SH2–peptide complex were calculated from the explicitly solvated MD trajectories. The energy of the group (*E*<sub>grp</sub>) was determined from the sum of the internal energy (*E*<sub>internal</sub>), which includes the molecular mechanics energy for the bonded and nonbonded interactions associated with the atoms of the group, and one-half the nonbonded energies for the interactions of the group with other water molecules (*E*<sub>solvent</sub>) and with protein or peptide atoms (*E*<sub>solute</sub>).

$$E_{\text{grp}} = E_{\text{internal}} + 0.5E_{\text{solvent}} + 0.5E_{\text{solute}} \quad (2)$$

Interaction energies were averaged over the 2 ns simulation time period using snapshots every 1 ps.

- (39) Jung, Y.-S. Z. M. *J. Biomol. NMR* **2004**, *30*, 11–23.  
 (40) Muhandiram, D. R.; Kay, L. E. *J. Magn. Reson.* **1994**, *103*, 203–216.  
 (41) Taylor, J. D.; Fawaz, R. R.; Ababou, A.; Williams, M. A.; Ladbury, J. E. *J. Biomol. NMR* **2005**, *32*, 339.  
 (42) Farrow, N. A.; Muhandiram, R.; Singer, A. U.; Pascal, S. M.; Kay, C. M.; Gish, G.; Shoelson, S. E.; Pawson, T.; Forman-Kay, J. D.; Kay, L. E. *Biochemistry* **1994**, *33*, 5984–6003.  
 (43) Schleucher, J.; Schwendinger, M.; Sattler, M.; Schmidt, P.; Schedletsky, O.; Glaser, S. J.; Sørensen, O. W.; Griesinger, C. *J. Mol. Biol.* **1994**, *4*, 301–306.  
 (44) Garrett, D. S.; Seok, Y.-J.; Peterkofsky, A.; Clore, G. M.; Gronenborn, A. M. *Biochemistry* **1997**, *36*, 4393–4398.  
 (45) Brooks, B. R.; et al. *J. Comput. Chem.* **2009**, *30*, 1545–1614.  
 (46) MacKerell, A., Jr.; Bashford, D.; Bellott, M.; Dunbrack, R., Jr.; Evanseck, J.; Field, M.; Fischer, S.; Gao, J.; Guo, H.; Ha, S. *J. Phys. Chem. B* **1998**, *102*, 3586–3616.  
 (47) MacKerell, A. D., Jr.; Feig, M.; Brooks, C. L., III. *J. Comput. Chem.* **2004**, *25*, 1400–1415.

- (48) Johnson, R. D., III, Ed. NIST Computational Chemistry Comparison and Benchmark Database, NIST Standard Reference Database Number 101, Release 14, September, 2006; <http://srdata.nist.gov/cccbdb>.  
 (49) Waksman, G.; Shoelson, S. E.; Pant, N.; Cowburn, D.; Kuriyan, J. *Cell* **1993**, *72*, 779–790.  
 (50) Caves, L. S. D.; Evanseck, J. D.; Karplus, M. *Protein Sci.* **1998**, *7*, 649–666.  
 (51) Shen, Y.; Bax, A. *J. Biomol. NMR* **2007**, *38*, 289–302.  
 (52) De Loof, H.; Nilsson, L.; Rigler, R. *J. Am. Chem. Soc.* **1992**, *114*, 4028–4035.

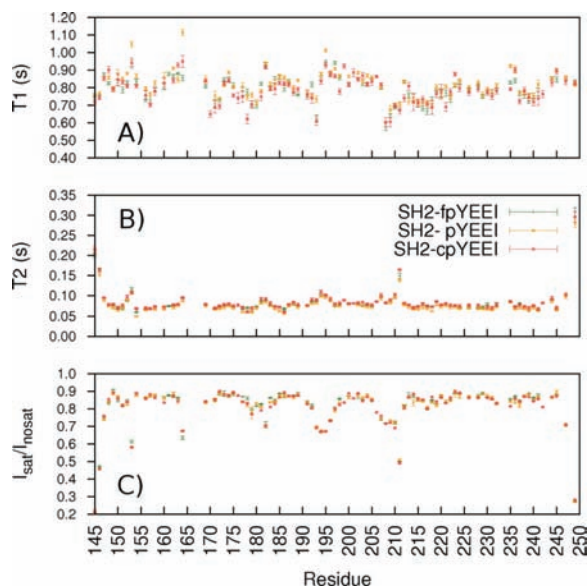


**Figure 2.**  $^{15}\text{N}$  (A)  $T_1$ , (B)  $T_2$ , and (C) heteronuclear NOE ( $I_{\text{sat}}/I_{\text{nosat}}$ ) relaxation values, measured at 18.8 T for the Src SH2–fpYEEI (green), Src SH2–pYEEI (gold), and Src SH2–cpYEEI (red) complexes.

Networks of water molecules identified from several crystallographic structures of Src SH2–peptide complexes<sup>3,14</sup> are thought to stabilize the bound state. The occupancy and energetics of these networks were characterized from the MD trajectories. One site,  $W_{\text{G236}}$ , refers to water molecules within 6.0 Å of non-hydrogen atoms of either residues G236 or L237 and within 6.0 Å of residue Y202. The second site,  $W_{+2E}$ , corresponds to water molecules within 3.2 Å of both protein residue R205 and peptide residue pY+2E as well as within 6.0 Å of the main-chain heavy atoms of both residues K203 and I214. (See Supporting Information Figure S1 for a graphical depiction of the water sites.) Occupancy was determined from the time average number of water molecules meeting these distance criteria for trajectory snapshots at 1 ps intervals. For each

group of water molecules selected, the time-averaged site energy was calculated using eq 2.

## Results

**Internal Dynamics Probed by NMR and MD.** To test for possible differences in internal dynamics of the Src SH2–pYEEI, Src SH2–cpYEEI, and Src SH2–fpYEEI complexes,  $^{15}\text{N}$  relaxation experiments were conducted for each complex.  $T_1$  and  $T_2$  relaxation times, and the  $^1\text{H}$ – $^{15}\text{N}$  heteronuclear NOE ( $I_{\text{sat}}/I_{\text{nosat}} - 1$ ), are sensitive to motions on a picosecond to nanosecond time scale, while  $T_2$  is also sensitive to longer time scale motion associated with conformational exchange. The residue profiles for these relaxation parameters are shown in Figure 2. For most residues, the values deviate among the complexes by an amount less than experimental error. The profiles show similar trends of relatively diminished  $I_{\text{sat}}/I_{\text{nosat}}$  and slightly elevated  $T_2$  values, indicating higher internal mobility, for residues N-terminal to the  $\alpha\text{A}$  helix (residue 153), in the AB (residue 164), CD (residues 192–195), and DE (residues 206–211) loop regions, and in the N and C termini. These relaxation data are thus remarkably similar between the complexes even in these more flexible loop regions. Rotational anisotropy manifests more strongly in  $T_1$  than in  $T_2$ , and therefore the observed  $T_1$  profiles in Figure 2 (top) are less uniform than those for  $T_2$  (middle). Small differences in  $T_1$  occur for residues scattered throughout the protein (I153, N164, E178, N193, D235). These  $T_1$  deviations range from 0.1 to 0.2 s and, based on Lipari–Szabo model-free theory,<sup>53</sup> reflect small differences in the amplitude of fast time scale motion, corresponding to a maximum disparity in the generalized order parameter of only  $\sim 0.2$ . Because these dynamic variations are small and occur for residues scattered throughout Src SH2, we find no convincing argument that they are relevant to the enthalpic differences of Src SH2 binding the three ligands. Overall, the NMR relaxation data suggest that Src SH2 main-chain fluctuations are highly similar and provide no evidence

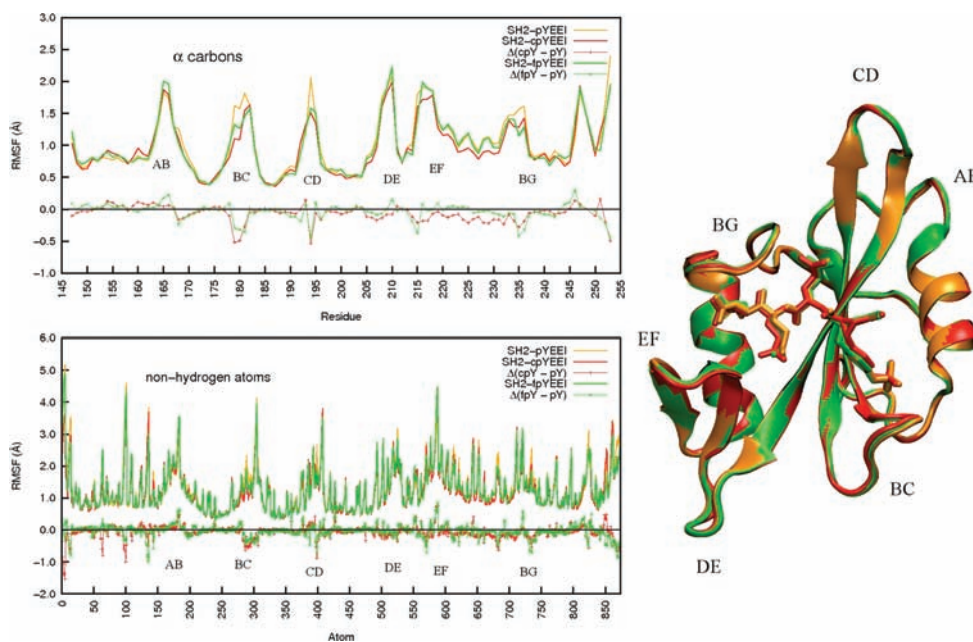


**Figure 3.** Root mean square fluctuations (RMSF) for  $\alpha$ -carbons (upper left) and non-hydrogen atoms (lower left) and overlaid average structures calculated from MD trajectories (right) of the Src SH2–pYEEI (gold), Src SH2–cpYEEI (red), and Src SH2–fpYEEI (green) complexes.  $\Delta(\text{cpY} - \text{pY})$  and  $\Delta(\text{fpY} - \text{pY})$  denote the differences of each analogue peptide complex with respect to the pYEEI complex. The flexible loops are labeled according to their topological nomenclature. Protein image was produced with VMD.<sup>79</sup>

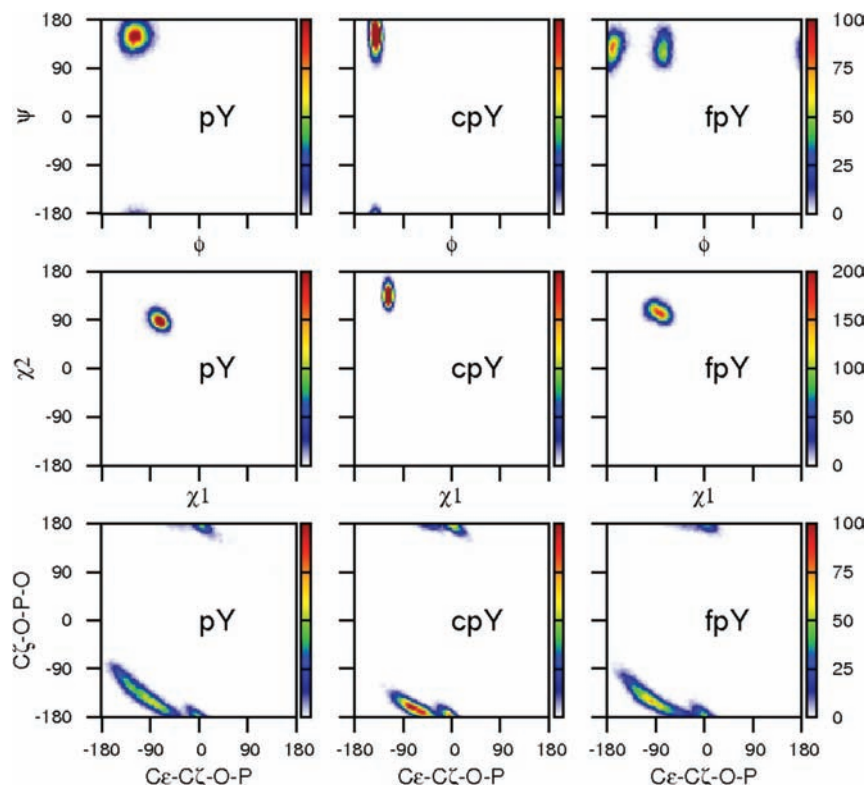


**Figure 4.** 2D histograms displaying  $\phi$ - $\Psi$ ,  $\chi_1$ - $\chi_2$ , and phosphate dihedral distributions for the pY, cpY, and fpY residues from MD simulations of each complex.

for conformational averaging that could account for variations in binding enthalpies upon association with pYEEI, fpYEEI, and cpYEEI.

The Src SH2–ligand complexes were also observed to have comparable positional fluctuations based on MD simulations. Protein root mean square fluctuations (RMSF) about the mean coordinates of the simulation, calculated over each 10 ns trajectory set (Figure 3), are nearly equal; the RMSF values for some loop residues vary up to  $\sim 0.5$  Å for the C $\alpha$  atoms (top) and up to  $\sim 0.9$  Å for a small number of non-hydrogen atoms (bottom). The greatest differences in RMSF are found for residues in the AB, BC, CD, and BG loops. Given their small magnitude and because these differences occur in mobile loop regions, which in general require longer sampling times for convergence, the disparities are not deemed sufficient to account for the variation in binding energetics.

The influence of the cyclopropyl constraint on the conformational distribution of the cpY residue as compared to pY and fpY was considered by examining the joint probability distributions for  $\phi$ - $\Psi$ ,  $\chi_1$ - $\chi_2$ , and dihedral angles describing rotation of the phosphoryl group (Figure 4). The peaks in the two-dimensional histograms for cpY are sharper in  $\phi$  and  $\chi_1$  than those for pY or fpY, demonstrating the expected reduced range of motion (see also Table 1) for the constrained ring. Interestingly, the constraint also has long-distance effects on the dihedral angles about the bridging oxygen of the phosphoryl group (bottom plots, Figure 4); the distribution for C $\zeta$ -O $\eta$ -P-O is narrower for cpY as compared to fpY and pY (Table 1).

Much like the trend between the crystal structures, the average coordinates of the complexes calculated from the simulation trajectories are strikingly similar to each other (Figure 3, right).

**Table 1.** Crystallographic and Simulated Geometries for pY, cpY, and fpY in the Respective Ligand Complexes with v-Src SH2, and for +1 E  $\phi$

dihedral (deg)	Src SH2–pYEEI	Src SH2–cpYEEI	Src SH2–fpYEEI
$\phi$ (X-ray) <sup>a</sup>	-116.3 (7.4)	-136.9 (2.3)	
$\phi$ (MD) <sup>b</sup>	-116.3 (14.6)	-138.9 (5.3)	-129.5 (46.3)
$\Psi$ (X-ray) <sup>a</sup>	143.7 (6.9)	146.3 (5.6)	
$\Psi$ (MD) <sup>b</sup>	151.0 (15.8)	150.9 (18.5)	128.5 (18.8)
$\chi_1$ (X-ray) <sup>a</sup>	-72.6 (7.1)	-116.2 (0.8)	
$\chi_1$ (MD) <sup>b</sup>	-72.1 (9.8)	-116.0 (4.2)	-83.2 (12.5)
$\chi_2$ (X-ray) <sup>a</sup>	83.6 (19.0)	134.0 (1.9)	
$\chi_2$ (MD) <sup>b</sup>	90.5 (10.4)	137.3 (12.5)	106.1 (10.8)
C $\epsilon$ -C $\zeta$ -O-P (X-ray) <sup>a</sup>	-75.6 (19.5)	-69.7 (4.8)	
C $\epsilon$ -C $\zeta$ -O-P (MD) <sup>b</sup>	-78.1 (53.4)	-46.7 (-36.0)	-74.4 (48.4)
C $\zeta$ -O $\eta$ -P-O (X-ray) <sup>a</sup>	-137.6 (6.3)	-167.4 (3.5)	
C $\zeta$ -O $\eta$ -P-O (MD) <sup>b</sup>	-146.1 (30.0)	-166.7 (14.7)	-151.8 (23.3)
pY+1 E $\phi$ (X-ray) <sup>a</sup>	-79.4 (11.1)	-63.9 (1.7)	
pY+1 E $\phi$ (MD) <sup>b</sup>	-94.5 (19.6)	-85.4 (20.7)	-86.4 (18.3)

<sup>a</sup> Standard deviation over multiple crystallographic chains in parentheses. <sup>b</sup> Standard deviation over MD snapshots in parentheses.

The three complexes differ from each other by  $\sim 0.7$  Å over main-chain atoms and  $\sim 1$  Å rmsd over all non-hydrogen atoms. In regard to the pY residue itself, the average values for  $\chi_1$ ,  $\chi_2$ , and phosphate dihedral angle, as well as  $\phi$  for residue Y+1 E, only two bonds removed from the point of constraint, differ by as much as 15° among the three bound ligands in both the crystallographic and the MD structures (Table 1). These structural differences may seem large, but the rotation of the phosphate group is able to orient the ring so that strong interactions and the position of the phosphotyrosyl moiety appear to be maintained with respect to the protein.

**Chemical Shift Perturbation Analysis.** Chemical shift is an exquisitely sensitive probe of local structure and magnetic environment. In contrast to the similarities observed for the

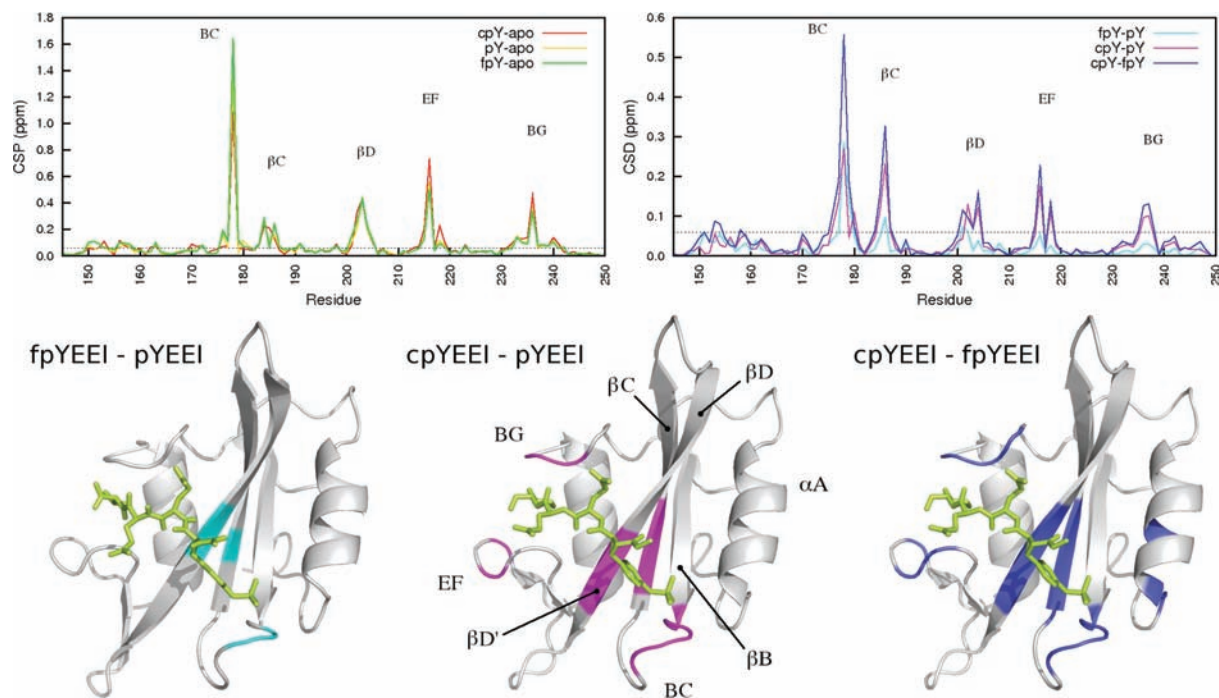


**Figure 5.** Chemical shift perturbations (CSPs) (upper left) and chemical shift differences (CSDs) (upper right) plotted as a function of residue number. The horizontal dashed line on each plot shows the 0.06 ppm ( $2^*(Iw)$ ) cutoff used to select for perturbed residues. CSDs between the Src SH2–fpYEEI and Src SH2–pYEEI complexes (cyan, lower left), Src SH2–cpYEEI and Src SH2–pYEEI complexes (magenta, lower center), and Src SH2–cpYEEI and Src SH2–fpYEEI (blue, lower right) are mapped onto the crystal structures. Protein images were produced with VMD.<sup>79</sup>

crystallographic and MD average structures, the  $^1\text{H}$ – $^{15}\text{N}$  HSQC spectra of the unbound Src SH2 domain and the three complexes exhibit numerous differences, which indicate that experimentally measurable structural variations do exist. To assess the spectral differences, chemical shift perturbations (CSP) were calculated for each complex relative to the unbound spectrum (Figure 5, upper left), and chemical shift differences (CSD) were calculated between each complex (Figure 5, upper right). CSP values greater than 0.1 ppm are typically considered indicative of significant binding effects,<sup>34,54–57</sup> whereas values greater than 0.2 ppm indicate highly shifted CSP values.<sup>54,55</sup> The main-chain amide resonances of Src SH2 are especially sensitive to ligand binding, and a number of CSPs are greater than 0.3 ppm (Figure 5, upper left). A similar profile was reported for v-Src SH2 binding to a longer variant of pYEEI.<sup>54</sup> The number of residues perturbed, as well as the magnitude of the differences, between the three complexes is remarkable in light of the degree of similarity between the crystal structures and simulation average structures.

While the CSP indicates a change in the electronic environment of the amide group upon ligand binding, the CSD more specifically compares the chemical shifts between complexes. The bulk of the discussion will therefore focus on the CSDs. Main-chain CSDs between the three complexes that are greater than 0.06 ppm, a value greater than twice the average peak line width in the spectra, are mapped onto the structure in the lower panel of Figure 5 and tabulated in Table S1 (Supporting

Information). The chemical shifts of Src SH2 bound with the constrained cpYEEI deviate significantly from those of the other two complexes, as highlighted by the extent of the magenta (lower center) and blue (lower right) mappings. The SH2–pYEEI and SH2–fpYEEI complexes are more similar to each other, as illustrated by the relative sparsity of the cyan mapping (lower left).

Ligand-dependent chemical shift differences are scattered across the binding interface, but are most prominent in the BC loop, the  $\beta\text{C}$  and  $\beta\text{D}$  strands of the central  $\beta$  sheet, the EF loop, and the BG loop (Figure 5). The perturbed residues of the BC loop and a portion of the residues in  $\beta\text{C}$  and  $\beta\text{D}$  form part of the highly conserved pY-binding pocket. The remaining perturbed residues in  $\beta\text{C}$  and  $\beta\text{D}$ , along with the EF and BG loops, contribute to the specificity-determining region, interacting with the EEI motif. Throughout this report, the secondary structural elements will be referred to by the standard SH2 topological nomenclature defined by Eck et al.<sup>58</sup> Residues will be referenced according to Src kinase numbering, and residue names in parentheses cross-reference the topological names that appear in the SH2 literature.

The greatest chemical shift differences between the three complexes are associated with residues directly involved with pY binding (see Table S1): E178 (GluBC1) main-chain amide ( $\text{CSD}_{\text{fpY-pY}} = 0.278$ ,  $\text{CSD}_{\text{cpY-pY}} = 0.281$ ,  $\text{CSD}_{\text{cpY-fpY}} = 0.558$  ppm) and R175 (Arg $\beta\text{B5}$ ) side-chain guanidinium  $\text{N}\eta\text{H}\eta$  ( $\text{CSD}_{\text{fpY-pY}} = 0.255$ ,  $\text{CSD}_{\text{cpY-pY}} = 0.332$ ,  $\text{CSD}_{\text{cpY-fpY}} = 0.586$  ppm). Figure 6 highlights these perturbations with four overlaid  $^1\text{H}$ – $^{15}\text{N}$  HSQC spectra for the unligated Src SH2 and the three complexes. Of particular interest is the observation that the trend in chemical shift perturbation follows the rank order of the binding enthalpies; the fpYEEI complex (green peaks) is the

(54) Taylor, J. D.; Ababou, A.; Fawaz, R. R.; Hobbs, C. J.; Williams, M. A.; Ladbury, J. E. *Proteins* **2008**, *73*, 929–940.

(55) Williamson, R. A.; Carr, M. D.; Frenkiel, T. A.; Feeney, J.; Freedman, R. B. *Biochemistry* **1997**, *36*, 13882–13889.

(56) Ma, J.; Gruschus, J. M.; Tjandra, N. *J. Am. Chem. Soc.* **2009**, *131*, 9884–9885.

(57) Groesch, T.; Zhou, F.; Mattila, S.; Geahlen, R.; Post, C. *J. Mol. Biol.* **2006**, *356*, 1222–1236.

(58) Eck, M. J.; Shoelson, S. E.; Harrison, S. C. *Nature* **1993**, *362*, 87–91.

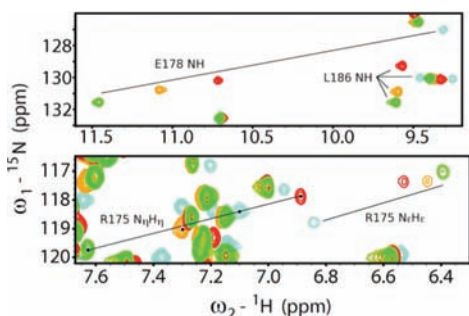


**Figure 6.** Overlay of  $^{15}\text{N}$  HSQC spectra of the unbound Src SH2 (cyan), Src SH2–cpYEEI complex (red), Src SH2–pYEEI complex (gold), and Src SH2–fpYEEI complex (green) featuring E178 NH, L186 NH, R175 N $\eta$ H $\eta$ , and R175 N $\eta$ H $\eta$ .

most enthalpically stable complex and has the most downfield (larger ppm) chemical shifts, while the cpYEEI complex (red peaks) is the least enthalpically stable complex and has the most upfield (smaller ppm) chemical shifts of the three complexes. The higher frequency of a downfield shifted resonance indicates the proton is relatively deshielded, which in proteins typically arises from stronger hydrogen bonding. As depicted in Figure 7, the E178 main-chain amide nitrogen is within hydrogen-bonding distance ( $\sim 2.8$  Å) of the nearest phosphate oxygen in the crystal structures. R175, which is universally conserved across SH2 domains, forms a bidentate salt-bridge with the phosphate group as well as hydrogen bonds to the side-chains of H201 (His $\beta$ D4) and S187 (Ser $\beta$ C5). Although R175 side-chain resonances exhibit large CSD values, no significant differences are observed for R175 main-chain chemical shifts. Appreciable main-chain amide CSDs between all complexes are found for S177 (Ser $\beta$ B7), T179 (ThrBC2), and C185 (Cys $\beta$ C3), all of which have side-chain interactions with the phosphoryl group. The remaining interactions responsible for coordinating the pY side-chain are mediated through the long, basic side-chains of R155 (Arg $\alpha$ A2) and K203 (Lys $\beta$ D6). Of these two residues, only K203 shows a significant main-chain CSD in the constrained pseudopeptide complex.

In addition to the  $\beta$ -sheet residues R175 and C185 just discussed, the chemical shifts of the central  $\beta$  sheet residues L186 (Leu $\beta$ C4), H201 (His $\beta$ D4), Y202 (Tyr $\beta$ D5), and I204 (Ile $\beta$ D7) differ considerably among the three complexes (Figure 5). The second largest CSDs are observed for the central  $\beta$ C strand residue L186 ( $\text{CSD}_{\text{fpY-pY}} = 0.095$ ,  $\text{CSD}_{\text{cpY-pY}} = 0.231$ ,  $\text{CSD}_{\text{cpY-fpY}} = 0.326$  ppm, Figures 5 and 6). Such large differences are unexpected, as L186 makes neither direct contacts nor apparent conformational changes between complexes based on the crystal structures. The differences are greater than those in neighboring residues, C185 ( $\text{CSD}_{\text{fpY-pY}} = 0.047$ ,  $\text{CSD}_{\text{cpY-pY}} = 0.112$ ,  $\text{CSD}_{\text{cpY-fpY}} = 0.155$  ppm) and S187 ( $\text{CSD}_{\text{fpY-pY}} = 0.008$ ,  $\text{CSD}_{\text{cpY-pY}} = 0.065$ ,  $\text{CSD}_{\text{cpY-fpY}} = 0.072$  ppm), or in R175, all of which contribute directly to the network of interactions in the pY-binding pocket (Figure 7). The C185 and S187 main-chain chemical shifts differ only in the comparisons to the constrained complex, while the shifts in both the pYEEI and the fpYEEI complexes are similar. Y202 ( $\text{CSD}_{\text{fpY-pY}} = 0.065$ ,  $\text{CSD}_{\text{cpY-pY}} = 0.129$ ,  $\text{CSD}_{\text{cpY-fpY}} = 0.096$  ppm) forms main-chain  $\beta$ -sheet hydrogen bonds to L186, as well as energetically important side-chain contacts with the Y+1 E residue of the peptide and the hydrophobic binding pocket.

The HN resonance for H201 had large CSD values at saturation ( $\text{CSD}_{\text{fpY-pY}} = 0.072$ ,  $\text{CSD}_{\text{cpY-pY}} = 0.049$ ,  $\text{CSD}_{\text{cpY-fpY}} = 0.116$  ppm). Moreover, the trend in the H201 amide proton

chemical shifts follows the rank order of the binding enthalpies in the same manner as detailed above for E178 NH and R175 N $\eta$ H $\eta$ . That is, the shift for the most enthalpically stable SH2–fpYEEI complex is furthest downfield ( $\delta_{\text{H}} = 8.443$  ppm), and that for the least enthalpically stable SH2–cpYEEI complex is furthest upfield ( $\delta_{\text{H}} = 8.284$  ppm), with the SH2–pYEEI complex being intermediate ( $\delta_{\text{H}} = 8.353$ ). The more downfield chemical shift indicates greater deshielding and suggests stronger H201 HN hydrogen-bonding interactions for the SH2–cpYEEI complex. The H201 amide also showed a unique titration behavior; the H201 peak was absent in the SH2–cpYEEI complex spectra at pseudopeptide to protein molar ratios as high as 2.5 (data not shown). This broadening for the cpYEEI complex indicates a possible chemical exchange process that is exhibited by neither pYEEI nor fpYEEI complexes (see Discussion). Because of spectral overlap of the H201 peaks, reliable  $^{15}\text{N}$ -relaxation measurements could not be obtained for H201 in any of the three complexes, and thus the exchange process was not further characterized.

The effects of preorganization also extend into the hydrophobic binding pocket as shown by large CSDs involving the cpYEEI complex for residues in the  $\beta$ D strand and the BG and EF loops. The L186 side-chain is a central component of this pocket, packing with the side-chains of Y202, I204 (Ile $\beta$ D7) ( $\text{CSD}_{\text{fpY-pY}} = 0.042$ ,  $\text{CSD}_{\text{cpY-pY}} = 0.114$ ,  $\text{CSD}_{\text{cpY-fpY}} = 0.156$  ppm), and L237 (LeuBG4) ( $\text{CSD}_{\text{fpY-pY}} = 0.030$ ,  $\text{CSD}_{\text{cpY-pY}} = 0.100$ ,  $\text{CSD}_{\text{cp-fpY}} = 0.129$  ppm). The chemical shifts of the EF and BG loops are also very responsive to peptide binding; S216 (SerEF $^2$ ) ( $\text{CSD}_{\text{fpY-pY}} = 0.053$ ,  $\text{CSD}_{\text{cpY-pY}} = 0.174$ ,  $\text{CSD}_{\text{cpY-fpY}} = 0.227$  ppm) and T218 (Ile $\beta$ F1) ( $\text{CSD}_{\text{fpY-pY}} = 0.030$ ,  $\text{CSD}_{\text{cpY-pY}} = 0.108$ ,  $\text{CSD}_{\text{cpY-fpY}} = 0.137$  ppm) of the EF turn, and G236 (GlyBG3) ( $\text{CSD}_{\text{fpY-pY}} = 0.027$ ,  $\text{CSD}_{\text{cpY-pY}} = 0.101$ ,  $\text{CSD}_{\text{cpY-fpY}} = 0.128$  ppm) of the BG loop show large CSDs in the constrained complex (Figure 5, Table S1) despite their lack of direct association with the peptide. S216 CSPs are dominated by changes in the  $^{15}\text{N}$  frequency and show the second largest CSPs upon binding all three ligands ( $\text{CSP}_{\text{pY}} = 0.562$ ,  $\text{CSP}_{\text{cpY}} = 0.734$ ,  $\text{CSP}_{\text{fpY}} = 0.509$  ppm) (Figure 5, top left).

**MD Analysis of Intermolecular Interactions.** To gain insight into the basis for the differences in binding enthalpy, we evaluated the particular intermolecular interactions of the residues that exhibit large CSD values from MD simulations. E178 NH and R175 N $\eta$ H $\eta$ , which show the largest CSD values, interact directly with the phosphoryl group of the constrained residue. The time-averaged number of hydrogen bonds per snapshot, the nonbond energy of interaction for the groups containing the respective donor and acceptor atoms, and the distances (oxygen to hydrogen, or oxygen to nitrogen) for these interactions vary little among the three complexes (Table 2). A higher energy is observed for R175 N $\eta$ H $\eta$  interaction with the phosphoryl group in the cpYEEI SH2 complex ( $-135.8$  versus  $-136.7$  or  $-136.9$  kcal/mol), consistent with this complex having the least favorable binding enthalpy. The outer  $\beta$ D strand residues H201 and Y202 also have large main-chain amide CSDs. The main-chain carbonyl of H201 forms a hydrogen bond to the NH group of residue Y+1 E, as illustrated in Figure 7. The average nonbond energy between Y+1 NH and H201 CO in the SH2–cpYEEI complex ( $-1.8$  kcal/mol) is higher than that in either SH2–pYEEI ( $-2.8$  kcal/mol) or SH2–fpYEEI ( $-2.6$  kcal/mol) as the result of an increase in the N $_H$ –O distance, and a corresponding smaller fraction of snapshots that fit the hydrogen-bonding criteria (Table 2). The differences in the interaction energies are smaller than the standard error.



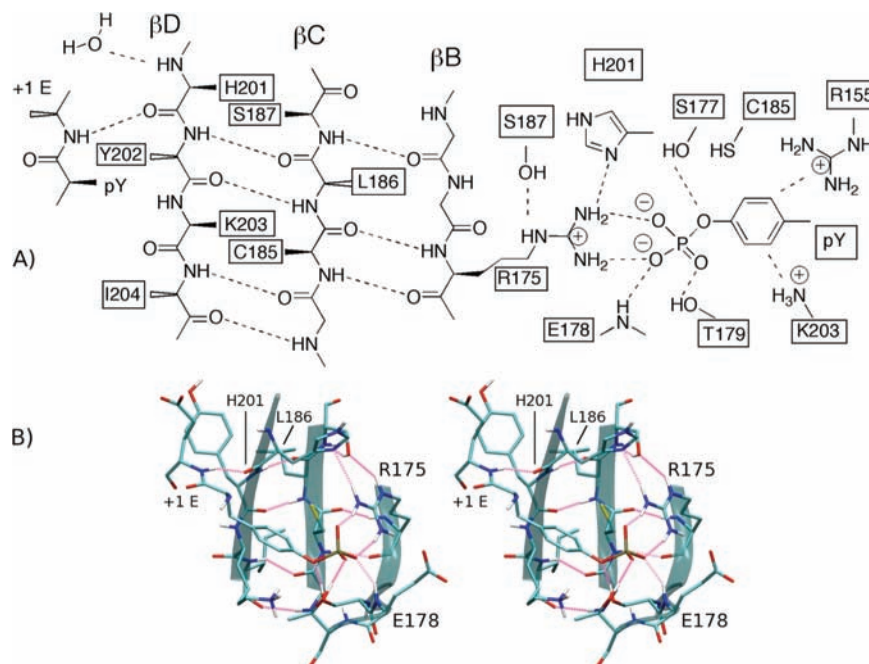


**Figure 7.** (A) Schematic view of the pY-binding pocket and central  $\beta$ -strands highlighting key residues showing chemical shift differences. Residues labeled with solid wedges extend from the  $\beta$ -sheet into the pY-binding pocket, while residues labeled with open wedges extend into the hydrophobic binding pocket. Dashed lines represent hydrogen bonds and salt-bridging interactions. (B) Stereoview of the pY-pocket interactions and central  $\beta$ -sheet. Hydrogen bonds are highlighted in pink. Protein image was produced with VMD.<sup>79</sup>

**Table 2.** Geometric and Energetic Analyses from MD for Interactions of Residues with Large CSD and a Trend in  $^1\text{H}$  NMR Frequencies Following the Rank Order in the Binding Enthalpy of the Three Complexes

	Src SH2-pYEEI	Src SH2-cpYEEI	Src SH2-fpYEEI
R175 N $\eta_1$ -H $\eta_{11}$ --O-P			
$\langle\text{H-bond}\rangle^a$	2.082	2.100	2.078
$\langle\text{Ener}\rangle^c$	-136.9 (6.0)	-135.8 (6.7)	-136.7 (5.8)
$\langle r_{\text{NO}}\rangle^b$	2.69 (0.11)	2.67 (0.10)	2.68 (0.11)
E178 N-H--O-P			
$\langle\text{H-bond}\rangle^a$	0.984	1.001	0.895
$\langle\text{Ener}\rangle^c$	-11.9 (0.4)	-11.7 (0.4)	-10.8 (2.9)
$\langle r_{\text{HO}}\rangle^b$	1.86 (0.19)	1.83 (0.14)	2.04 (0.63)
$\langle r_{\text{NO}}\rangle^b$	2.82 (0.17)	2.78 (0.13)	2.97 (0.58)
+1 E N-H--O=C H201			
$\langle\text{H-bond}\rangle^a$	0.889	0.586	0.876
$\langle\text{Ener}\rangle^c$	-2.8 (0.1)	-1.8 (1.0)	-2.6 (0.2)
$\langle r_{\text{HO}}\rangle^b$	2.03 (0.20)	2.65 (0.84)	2.10 (0.28)
$\langle r_{\text{NO}}\rangle^b$	2.97 (0.18)	3.49 (0.73)	3.02 (0.23)

<sup>a</sup> Average number of hydrogen bonds per snapshot. <sup>b</sup> Average distance ( $\text{\AA}$ ) with standard error in parentheses. <sup>c</sup> Average nonbonded energy (kcal/mol) between xpY(C $\zeta$ -O-PO $_3$ ) and R175(N $\eta_1$ H $\eta_{11}$ H $\eta_{12}$ N $\eta_{22}$ -H $\eta_{21}$ H $\eta_{22}$ C $\zeta$ N $\epsilon$ H $\epsilon$ ). <sup>d</sup> Average nonbonded energy (kcal/mol) between xpY(C $\zeta$ -O-PO $_3$ ) and E178(H $\eta_1$ N $\alpha$ H $\alpha$ ). <sup>e</sup> Average nonbonded energy (kcal/mol) between xpY+1(H $\eta_1$ N $\alpha$ H $\alpha$ ) and Y202(OC).

Nevertheless, the overall tendency of the simulation results in Table 2 is that the interactions with ligand of R175 and H201, residues with a rank-order chemical shift trend for the three complexes, are somewhat less favorable for the cpYEEI complex, consistent with the measured enthalpic differences.

A number of interfacial water molecules are observed in the crystal structures to mediate interactions between the peptide and SH2 domain and appear to be energetically important to the stability of the complex.<sup>3,14,73-75</sup> Waksman and co-workers found a significant improvement in the agreement of binding enthalpies predicted using an empirical formulation based on surface area when these water molecules were included in the

**Table 3.** Energetic Contributions to Complex Stability in the Specificity-Determining Region<sup>a</sup>

	Src SH2-pYEEI	Src SH2-cpYEEI	Src SH2-fpYEEI
$W_{\text{G236}} \langle N \rangle$	4.4 (0.2)	4.7 (0.2)	4.4 (0.1)
$W_{\text{G236}} \langle E \rangle$	-10.9 (0.08)	-10.8 (0.05)	-10.8 (0.03)
$W_{+2E} \langle N \rangle$	3.6 (0.3)	3.9 (0.3)	3.3 (0.3)
$W_{+2E} \langle E \rangle$	-10.8 (0.08)	-10.5 (0.07)	-10.9 (0.11)

<sup>a</sup> Energies ( $\pm$ standard error) in kcal/mol, calculated according to eq 2. See Materials and Methods for definition of solvation sites, and Supporting Information for illustration of the sites;  $\langle N \rangle$  is the time-averaged number of water molecules ( $\pm$ standard error) occupying the site, and  $\langle E \rangle$  is the average energy per water molecule ( $\pm$ standard error) in kcal/mol.

estimate of surface area.<sup>73-75</sup> The possibility that hydration effects resulting from these interfacial water molecules differ among the three complexes was considered by using the MD trajectories to assess the occupancy and interaction energies of the water molecules in the sites identified by Waksman. One of these water molecules hydrogen bonds with the H201 NH group as shown in Figure 7. Analysis of the MD trajectories found the constrained pseudopeptide did not significantly change the occupancy for the constrained pseudopeptide as determined by the fraction of frames with a hydrogen bond between H201 NH and a water molecule (0.935 for SH2-pYEEI, 0.919 for SH2-cpYEEI, and 0.917 for SH2-fpYEEI). We also analyzed two clusters of interfacial water molecules present in several crystal structures. One cluster of approximately four water molecules lies near the pY+2E side-chain ( $W_{+2E}$ ). A second cluster, with roughly three water molecules, bridges interactions of G236 in the BG loop and the hydrophobic binding pocket ( $W_{\text{G236}}$ ) with the ligand. The time-averaged interaction energies calculated with eq 2 and number of water molecules in the site  $W_{+2E}$  and  $W_{\text{G236}}$  are nearly identical (Table 3). Explicit-water MD simulations provide information on hydration effects at a level of detail that is not obtained by experiment; however, it should be noted that the energetics of water interactions are

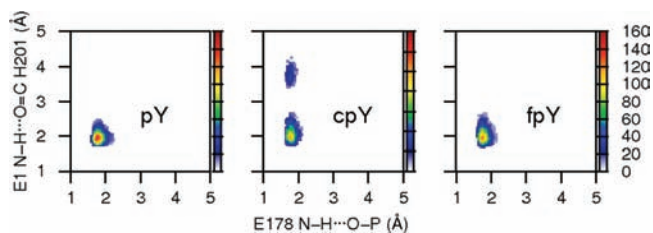


**Figure 8.** 2D histograms from MD simulations for the ligand–protein distances for (left) Src SH2–pYEEI, (center) Src SH2–cpYEEI, and (right) Src SH2–fpYEEI. The distance between the amide hydrogen atom of ligand residue Y+1 E and the carbonyl oxygen of H201 (His $\beta$ D4) is plotted along the y-axis. The distance between the main-chain amide proton of E178 (GluBC1) and the nearest phosphate oxygen atom is plotted along the x-axis.

difficult to quantify with high accuracy because of the limitations of the water models and the long simulation times required to reach absolute convergence. With this limitation in mind, the results shown in Table 3 give no indication that the interfacial water molecules differ significantly as a result of the cpY constraint.

An aim of this investigation was to explore the possibility that concerted atomic motions modulate noncovalent interactions in a manner that could explain the differences in binding enthalpies observed experimentally. Concerted motions include local motions such as libration of a functional group, or a collective motion of several groups across a network of interactions as is important for driving protein allostery and other conformational changes.<sup>59,60</sup> Consider that motion of the phosphotyrosyl residue optimizes the orientation of the phosphoryl group with respect to E178 and R175. Rigidity arising from the cpY main-chain constraint could hinder the ligand from concurrently maintaining stable main-chain hydrogen bonds between Y+1 E and H201. Two-dimensional histograms correlating the distance between E178 and the nearest phosphate oxygen atom with the Y+1 NH to H201 CO hydrogen-bond distance are shown in Figure 8. The distributions for the pYEEI complex and fpYEEI complex show a single well so that the ligand interactions with both E178 and H201 maintain a stable H–O distance of  $\sim 2$  Å, while the cpYEEI complex has a minor population of simulation snapshots with an increased Y+1 E to H201 distance of approximately 3.5–4 Å. This is manifested in the 0.6 Å increase in the mean Y+1 E H<sub>N</sub> to H201 O distance, decrease of 0.3 hydrogen bonds per frame, and 1 kcal/mol unfavorable change in interaction energy for cpYEEI listed in Table 2. These results suggest that the rigid constraint partly disrupts the pseudopeptide from simultaneously maintaining optimal interactions across the entirety of its binding interface.

## Discussion

The Src SH2 domain is a relatively rigid protein receptor with no induced-fit binding,<sup>14,35,49</sup> which makes it an attractive model system for ligand design, and simplifies the interpretation of ITC results and energetics of binding.<sup>13,14</sup> The structure of the Src SH2 domain appears unchanged in the unbound,<sup>54</sup> phosphate-bound,<sup>49</sup> pYEEI-bound,<sup>49</sup> and cpYEEI-bound<sup>14</sup> states, as well as in complexes with a variety of other pY-based

inhibitors.<sup>61</sup> The similarities are particularly striking within the pY-binding pocket. Despite this apparent structural rigidity, the association of preorganized ligands with Src SH2 occurs with less favorable enthalpy of binding, albeit the desired gain in entropy. This enthalpy–entropy compensation motivated this investigation of possible conformational averaging affects given that relative motion of the protein and constrained peptide could lead to fluctuations with increased hydrogen-bond lengths or more acute angles between donor and acceptor such that motional averaging would lead to higher hydrogen-bond energy. Nonetheless, the internal dynamics of the pYEEI, cpYEEI, and fpYEEI Src SH2 complexes estimated from <sup>15</sup>N relaxation (Figure 2) and MD fluctuations (Figure 3) show only minor variations, which cannot convincingly account for the observed disparities in binding enthalpy of the three complexes. Previously reported NMR relaxation measurements for Src SH2 also suggest that main-chain flexibility varies little upon binding the canonical pYEEI peptide, with only minimal differences from residues scattered throughout the protein in the amplitude of motion specified from the Lipari–Szabo order parameter.<sup>54</sup> As such, we find no evidence that alternative conformational distributions occurring from picosecond–nanosecond motions affect the time-average interaction energy with the three Src SH2 ligands. These results do not directly assess possible differences in slower time scale motions. Nevertheless, given that slower motions correspond to larger amplitude motions, and that large-amplitude motions, such as loop motions, would likely be manifest in the average structure determined by crystallography, the structural similarity of the Src SH2 complexes would argue against the possibility that differences in slower time scale motions exist for these complexes.

**Disruptions to pY–Pocket Interactions.** In contrast to the above observations, important deviations in the chemical shifts of pY–pocket residues among the Src SH2 complexes reveal key distinctions that can be rationalized in energetic terms. The strongest CSDs (Table S1) between all three complexes are associated with the side-chain N $\eta$ H $\eta$  of R175 and the main-chain NH of E178, which both interact directly with the phosphoryl group (Figure 7). NMR CSDs for these residues are consistent with small structural variations that can reasonably account for the measured enthalpy differences of the three complexes. Recall that previously reported mutagenesis and calorimetry studies (Table S1) indicate that phosphotyrosyl binding contributes approximately one-half of the binding free energy and is largely enthalpically driven.<sup>3,62,63</sup> The free energy for Src SH2 binding pYEEI is  $\sim 6$  kcal/mol more favorable relative to that of YEEI, with  $\Delta\Delta H^\circ \approx -4$  kcal/mol and  $T\Delta\Delta S^\circ \approx 2$  kcal/mol.<sup>62</sup> Interactions that contribute the majority of the binding free energy have become known as binding hot spots.<sup>64,65</sup> Hot-spot residues were found by mutagenesis to have considerably greater power in altering affinity than neighboring residues that also exist in the intermolecular contact surface.

The large downfield perturbations in the chemical shifts for R175 and E178 are consistent with a distance-dependent

(59) Amaro, R. E.; Sethi, A.; Myers, R. S.; Davisson, V. J.; Luthey-Schulten, Z. A. *Biochemistry* **2007**, *46*, 2156–2173.

(60) Sethi, A.; Eargle, J.; Black, A.; Luthey-Schulten, Z. *Proc. Natl. Acad. Sci. U.S.A.* **2009**, *106*, 6620–6625.

(61) Lange, G.; Lesuisse, D.; Deprez, P.; Schoot, B.; Loenze, P.; Bénard, D.; Marquette, J.-P.; Broto, P.; Sarubbi, E.; Mandine, E. *J. Med. Chem.* **2003**, *46*, 5184–5195.

(62) Bradshaw, J. M.; Mitaxov, V.; Waksman, G. *J. Mol. Biol.* **1999**, *293*, 971–985.

(63) Bradshaw, J. M.; Mitaxov, V.; Waksman, G. *J. Mol. Biol.* **2000**, *299*, 521–535.

(64) Dwyer, J. J.; Dwyer, M. A.; Kossiakoff, A. A. *Biochemistry* **2001**, *40*, 13491–13500.

(65) Clackson, T.; Wells, J. A. *Science* **1995**, *267*, 383–386.

deshielding of the NH nuclei by direct contact with the ligand dianionic phosphoryl group.<sup>34</sup> The NMR chemical shift depends strongly on distance to nearby charged, polar, or aromatic groups, thereby providing a useful probe of main-chain amide hydrogen bonding, which is otherwise difficult to test by common approaches such as single-site mutagenesis. The SH2–fpYEEI complex exhibits the most downfield proton chemical shifts for E178 H<sub>N</sub> and R175 H<sub>η</sub>, suggesting stronger interactions and therefore shorter phosphate–HN distances. The cpYEEI shifts are furthest upfield, consistent with the longest distances and least favorable energy. The rank order in chemical shifts of these protons (Figure 6) therefore correlates with the binding enthalpies of the peptide series, and this correlation is consistent with increasing distance for the interaction with fpY, pY, and cpY residues, respectively. The relationship between chemical shift and hydrogen-bond stabilization has been well established for protein secondary structure<sup>66,67</sup> and model compounds.<sup>67–69</sup> Ab initio calculations have suggested that changes in hydrogen-bonding distance of tenths of an angstrom are sufficient to perturb the chemical shift by more than 1 ppm.<sup>68–70</sup> Furthermore, a 0.1 Å change in the phosphoryl group distance to the E178 amide and R175 guanidinium groups alters the interaction energy by approximately 1 and 4 kcal/mol, respectively, based on the molecular mechanics force field (Supporting Information Figure S2). Thus, in the case of Src SH2 binding, the trends in chemical shift indicate that subtle deviations in the interaction distances for the phosphotyrosine with the SH2 pY–pocket residues, perhaps due to small geometric variations between cpY, pY, and fpY residues, can account for the observed differences in binding enthalpies of the complexes.

The crystal structures were unable to distinguish the three complexes in terms of the distances between the phosphate and HN of E178 or R175; however, a difference of tenths of angstroms to account for the CSD is comparable to the ~0.3 Å estimated coordinate error of a crystallographic model determined at 1.9 Å resolution.<sup>70</sup> Further, the simulations find less favorable interaction energy of R175 guanidinium for the cpYEEI complex, but the trends in interaction energies of E178 NH and R175 N<sub>η</sub>H<sub>η</sub> do not correlate with the interaction energy indicated from chemical shifts. The simulations therefore also appear unable to capture the subtle structural effects observed by NMR. A more accurate treatment of electrostatics by including polarization<sup>70</sup> in the molecular mechanics force field is likely required to correctly model the behavior of the charged phosphoryl group.

Interpretation of chemical shift perturbations in terms of thermodynamic parameters necessitates caution as chemical shift is sensitive to a number of structural and environmental factors.<sup>34,71</sup> A quantitative interpretation requires accurate chemical shift calculations and detailed structural information for the system. Further, binding enthalpy depends on the energy difference between the bound and unbound state, and the

difference between two complexes alone may not fully explain deviations in binding thermodynamics. It is reasonable that the high degree of structural similarity between the three ligands in this study would minimize any contribution from the free state of the ligands, and MD studies are underway to actually estimate the contribution from the free state. Nevertheless, the relative downfield changes in chemical shift for E178 H<sub>N</sub> and R175 H<sub>η</sub> (Figure 6) indicate stronger deshielding and electrostatic potential for interaction in the order of the Src complexes: fpYEEI > pYEEI > cpYEEI. Given the interactions observed crystallographically, we propose closer contact and more favorable noncovalent ligand interactions of the phosphoryl group with E178 NH and R175 N<sub>η</sub>H<sub>η</sub> in the same relative order, and these interactions are in part the basis for the observed ranking in experimental binding enthalpies.

The energetic importance of R175 to binding affinity and as part of the hot spot interaction is well established.<sup>49</sup> The residue is universally conserved across SH2 domains. The structural importance of the hydrogen bonding between R175 and H201 has been supported by the acidic pK<sub>a</sub> of H201 N<sub>δ</sub>, measured by NMR titration in Src SH2<sup>54</sup> and PLCγ.<sup>72</sup> A triad of hydrogen bonds between R175, H201, and E159 is argued to preorganize the R175 side-chain in its bound state geometry.<sup>54</sup> The R175A Src SH2 mutant binds pYEEI with significantly reduced binding enthalpy ( $\Delta\Delta G^\circ = 3.2$  kcal/mol,  $\Delta\Delta H^\circ = 4.1$  kcal/mol,  $T\Delta\Delta S^\circ = 0.9$  kcal/mol<sup>62</sup>). The noncovalent interactions of the R175 side-chain with S187, H201, and the pY residue (Figure 7) provide ample energetic potential so that alterations of R175 by different ligands could cause a 2.7 kcal/mol difference in binding enthalpy that is observed between cpYEEI and fpYEEI.<sup>14</sup>

The NMR chemical shift differences for residues 201–204 (Figure 5) also suggest variations in the interactions of the outer  $\beta$ D strand of Src SH2. As illustrated in Figure 7A, H201 has main-chain interactions with pY+1E and with a bound water molecule,<sup>14</sup> which has been shown to be energetically important in a series of computational investigations by Waksman and co-workers.<sup>73–75</sup> The simulations find that in the cpYEEI complex two populations exist for the distance of H201 carbonyl to pY+1E NH (Figure 8). This conformational averaging may be the origin of the chemical exchange line broadening exhibited by H201 NH during the titration of Src SH2 with cpYEEI, and lowers the stability of this interaction based on the energies calculated from the simulations (Table 2). Moreover, given that the trend in the chemical shifts of H201 HN follow the rank order of the binding enthalpies (see Results), H201 interactions could contribute to the loss of enthalpy with preorganization. Interestingly, this loss would be attributed to the presence of dynamic averaging for the restrained cpYEEI rather than a loss of mobility.

**Long-Range Effects of Constraint.** Unlike the large CSD values of NH groups that interact directly with the phosphoryl moiety of the ligand, a precise structural explanation for the large CSDs in the central  $\beta$ C-strand residue L186 is less clear. Chemical shift differences in this region of p85N SH2 upon

(66) Wagner, G.; Pardi, A.; Wuethrich, K. *J. Am. Chem. Soc.* **1983**, *105*, 5948–5949.

(67) Wishart, D. S.; Sykes, B. D.; Richards, F. M. *J. Mol. Biol.* **1991**, *222*, 311–333.

(68) Cui, Q.; Karplus, M. *J. Phys. Chem. B* **2000**, *104*, 3721–3743.

(69) Asakawa, N.; Sato, D.; Sakurai, M.; Inoue, Y. *J. Phys. Chem. A* **2000**, *104*, 2716–2723.

(70) Mandell, D. J.; Chorny, I.; Groban, E. S.; Wong, S. E.; Levine, E.; Rapp, C. S.; Jacobson, M. P. *J. Am. Chem. Soc.* **2007**, *129*, 820–827. Brünger, A. T. *Methods Enzymol.* **1996**, *277*, 366–396.

(71) Parker, L. L.; Houk, A. R.; Jensen, J. H. *J. Am. Chem. Soc.* **2006**, *128*, 9863–9872.

(72) Singer, A. U.; Forman-Kay, J. D. *Protein Sci.* **1997**, *6*, 1910–1919.

(73) De Fabritiis, G.; Geroult, S.; Coveney, P. V.; Waksman, G. *Proteins* **2008**, *72*, 1290–1297.

(74) Geroult, S.; Virdee, S.; Waksman, G. *Chem. Biol. Drug Des.* **2006**, *67*, 38–45.

(75) Geroult, S.; Hooda, M.; Virdee, S.; Waksman, G. *Chem. Biol. Drug Des.* **2007**, *70*, 87–99. Neal, S.; Nip, A. M.; Zhang, H.; Wishart, D. S. *J. Biomol. NMR* **2003**, *26*, 215–240.

**Table 4.** Values from MD Simulations for the Dihedral Angles with Potential To Affect the Nitrogen Chemical Shift of L186

	Src SH2–pYEEI	Src SH2–cpYEEI	Src SH2–fpYEEI
L186 Dihedrals			
L186 $\delta_N$ (ppm)	130.897	129.266	131.570
$\Psi$ (C185) <sup>a</sup>	–143 (3)	142 (3)	144 (2)
$\phi$ (L186) <sup>a</sup>	–106 (4)	–105 (4)	–107 (2)
$\chi_1$ (C185) <sup>a</sup>	–74 (43)	–95 (35)	–85 (41)

<sup>a</sup> Time-averaged value in degrees with standard errors in parentheses.

ligand binding were attributed to ring current effects,<sup>34</sup> but this explanation cannot account for the CSD observed in the Src complexes studied here given that L186 HN exhibits larger differences (0.7 to 2.3 ppm in  $\delta_N$ , 0 to 0.04 ppm in  $\delta_H$ ) but is more distant from surrounding aromatic rings so that the ring currents would be considerably smaller. Also,  $\delta_N$  is less susceptible to the influence of ring currents than  $\delta_H$ ,<sup>75</sup> and the nitrogen chemical shift dominates the L186 CSD (Figure 6). Nitrogen chemical shifts are more complex and thus complicated to calculate as compared to proton shifts, but they are particularly sensitive to changes in the  $\phi$  dihedral angle, as well as the  $\Psi$  and  $\chi_1$  torsion angles of the preceding residue,<sup>76</sup> C185 in this case. The trends in  $\Psi$ (C185),  $\phi$ (L186), and  $\chi_1$ (C185) that are tabulated in Table 4 agree qualitatively with the variations in nitrogen chemical shifts in that the SH2–pYEEI and SH2–fpYEEI values are more similar to each other than to SH2–cpYEEI. The dihedral angle differences are less than the standard deviation, but on the basis of this consistent trend we suggest the CSDs could arise from small deviations in main-chain conformation of the central  $\beta$  strands induced by the constraint.

If the CSDs arise from small disparities in  $\Psi$  and  $\chi_1$  torsion angles of residue 185 and in  $\eta$  of 186 in the  $\beta C$  strand, we suggest the enthalpic impact of this local structural perturbation is likely negligible. Nevertheless, the chemical shift perturbations along the length of the  $\beta C$  and  $\beta D$  strands (residues 185, 186, 201–204) could reflect thermodynamic consequences in view of a coupling between the two binding pockets shown from calorimetric measurements of binding enthalpies.<sup>77</sup> Using a series of pYEEI variants binding to Src SH2, Waksman and co-workers reported a significant nonadditivity between the pY+3 I residue, and either the pY+1 E (1.2 kcal/mol) or the pY+2 E (–1.6 kcal/mol) residues.<sup>77</sup> Long-distance effects are also apparent here from the disparate NH chemical shifts; S216 and T218 in the EF loop and G236 and L237 of the BG loop differ for the cpYEEI complex, whereas the complexes of the more flexible fpYEEI and pYEEI ligands have similar bound state chemical shifts (Figure 5). Long-range effects originating from the pY–pocket are also indicated by a recent comparison of Src SH2 crystallographic structures in the unbound state determined in the presence and absence of inorganic phosphate. A notable difference was the closing of the EF and BG loops in the solution structure without phosphate, leading to a less well-defined hydrophobic binding pocket.<sup>54</sup> We envision a pathway of correlated interactions starting with the side-chains of residues C185, S187, H201, and K203 on the pY face of the  $\beta$ -sheet (solid wedges in Figure 7) mediated through the hydrophobic-face  $\beta$ -sheet residues L186, Y202, and I204 (open wedges in Figure 7) to the BG loop via contacts between L186, Y202, and L237. While a structural path between the pY–pocket

and the EF and BG loops on the opposite side of the SH2 domain is readily mapped out for the residues with CSDs, an interpretation of the large CSD values of the EF and BG loop is not obviously associated with the measured enthalpic differences as was the case for the trends in chemical shift deshielding for residues in the pY–pocket.

## Conclusion

This report has detailed several interactions in the pY–pocket of the Src SH2 domain as a basis for enthalpy–entropy compensation of ligand binding by using a combination of information from NMR, MD simulations, crystallography, and calorimetry. From the perturbations observed in the chemical shifts of the Src pY–binding pocket, it is seen that addition of even a minor structural constraint is not a perfect mimic of the optimal geometry of binding. Small, almost “invisible” changes in the bound state geometry appear to impact the binding energetics. These studies suggest that constraining a portion of a flexible ligand involved in hot-spot interactions with Src SH2 might be the origin of the weaker binding enthalpy observed for cpYEEI relative to fpYEEI and pYEEI.

To preorganize ligands without such an enthalpic penalty, it would appear necessary to closely match the binding site geometry of Src SH2. Alternatively, the introduction of a geometric constraint elsewhere in the ligand could yield improved entropy from preorganization without an enthalpic penalty resulting from an imperfect match of the targeted bound state geometry. For example, preorganization of the pY+3 side-chain, which is energetically forgiving to conservative mutations,<sup>77,78</sup> could provide the same entropic gain achieved with cpY but without requiring an ideal match of binding site geometry to not diminish key interactions of a “hot-spot” region. In this context, it is notable, perhaps perplexing, that use of the same cyclopropane-derived replacement at pY led to enhanced binding enthalpies without the expected gain in binding entropies for a series of Grb2 SH2 binding phosphotyrosine analogues,<sup>10,11</sup> thereby underscoring the difficulty in predicting binding thermodynamics from structure.

We find no evidence in this study that the compensating contributions in the measured enthalpy–entropy components arise from the same physical basis, and thus enthalpy–entropy compensation is not an intrinsic property of preorganization. That is, the reduced mobility from preorganization of the ligand leads to a more favorable binding entropy, but this reduced ligand mobility does not appear to be the origin of the less favorable binding enthalpy through an effect of the restraint on the conformational dynamics. As well as can be determined from the <sup>15</sup>N relaxation measurements and MD simulations, protein internal dynamics are not significantly affected by the constrained ligand motion in a manner that accounts for energetic differences. The results therefore do not support the view that compensation occurs because the entropy and enthalpy are inexorably linked and therefore an unavoidable property of the system. Thus, achieving the anticipated gain in binding free energy by preorganization of ligand in the bound state conformation appears to remain a potentially viable design principle, although predicting whether ligand preorganization will have a favorable entropic and/or enthalpic consequence is problematic.

**Acknowledgment.** We thank the National Institutes of Health (GM 39478 and GM 84965), the National Science Foundation (CHE

(76) Le, H.; Oldfield, E. *J. Phys. Chem.* **1996**, *100*, 16423–16428.

(77) Bradshaw, J. M.; Waksman, G. *Biochemistry* **1999**, *38*, 5147–5154.

(78) Bradshaw, J. M.; Waksman, G. *Biochemistry* **1998**, *37*, 9083–9090.  
(79) Humphrey, W.; Dalke, A.; Schulten, K. *J. Mol. Graphics* **1996**, *14*, 33–38.

0750329), the Markey Center for Structural Biology, the Purdue University Center for Cancer Research (CA 23568), The Robert A. Welch Foundation (F-652), and the Norman Hackerman Advanced Research Program for their generous support of this research. J.M.W. was supported by NIH Biophysics Training Grant GM 08296. We also thank David Cramer and James Myslinski for help in preparing the fpYEEI and cpYEEI ligands.

**Supporting Information Available:** Complete list of authors for ref 45; Table S1, a compilation of CSP and CSD values for residues showing significant chemical shift changes, as well as

published relative binding thermodynamic parameters for relevant mutants; Figure S1, an illustration of interfacial water molecules in the hydrophobic binding pocket; Figure S2, a plot of the distance dependence of the phosphoryl interaction energy calculated from MD simulations; and information on the CHARMM force field topology and parameters for the cpY and fpY residues. This material is available free of charge via the Internet at <http://pubs.acs.org>.

JA910535J